The Scientific Temper (2022) Vol. 13 (2): 425-431

E-ISSN: 2231-6396, ISSN: 0976-8653

https://scientifictemper.com/

ORIGINAL RESEARCH

Satellite radiance assimilation using the 3D-var technique for the heavy rainfall over the Indian region

Shivali Kundan, Neha Verma, Zahid Nabi, Dinesh Kumar*

Abstract

The present study evaluates the impact of satellite radiance assimilation on the predictability of the WRF model. The 3D-VAR system of the WRF model was used to assimilate satellite radiance data at the initial condition. Four thunderstorm cases were considered, which occurred over Kolkata, India. A set of two numerical experiments, namely CNTL (no-assimilation) and SAT (satellite radiance assimilation), were carried out, and the WRF model was integrated for 24 hours. The assimilation of satellite radiance had improved the wind and moisture fields at the initial condition, which led to evolve the conducive atmosphere further. Results showed that even though thunderstorms are a small-scale system, assimilation of satellite radiance had shown significant improvement in the simulation of the location, evolution, and intensity of thunderstorms. Temporal evolution of surface parameters (such as 2-m temperature and rainfall) was closer to observation (AWS) in SAT experiment. Further, the SAT experiments were able to produce stronger updrafts/downdrafts and increased moisture content deep into the atmosphere. These findings suggest that satellite radiance data assimilation significantly impacts initial conditions, providing a conducive atmosphere.

Keywords: Severe thunderstorms, Mesoscale data assimilation, Satellite radiance.

INTRODUCTION

The prediction of severe thunderstorms has conventionally been considered a difficult task due to the inherent non-linearity of their dynamics and physics (Orlanski, 1975). The difference between the scale of clouds and the resolution of the numerical weather prediction (NWP) models further complicated the problem. The horizontal scales of clouds are about a few kilometers, while the typical scales of the early NWP models were a few hundred kilometers. Mesoscale models are now available with wide flexibilities of changing horizontal and vertical resolution, nesting domains and choosing options for different physical parameterization schemes. With the advancement of computational resources, model resolution for simulation has become significantly finer. The present state-of-the-art high-resolution mesoscale models could provide better prediction of these systems to a certain extent. Mukhopadhyay (2004) performed an idealized simulation of thunderstorms using a regional atmospheric modeling system (RAMS) and demonstrated the requirement for high-resolution regional models. He found that the finer domain of 1km grid resolution simulated the severe convection associated with localized thunderstorms very close to observation as compared to the coarser domain of 5 Km grid resolution. Since the initial condition is the key element for accurate numerical weather prediction (NWP) (Lewis *et al.*, 1985); (Talagrand and Courtier, 1987), obtaining more realistic initial conditions becomes a challenging task for researchers and forecasters. Johns *et al.* (1992) reviewed the advancement in the methodology used for the forecasting of local severe thunderstorms at the national severe storms forecasting center (NSSFC) and discussed the improvement in the forecast of a numerical model with the assimilation of wind profiles and Doppler radars in real-time forecasts. Conventional (RS/RW, AWS, synop, Airport observations, etc.) and non-conventional observations, such as satellite radiance, can be combined by data assimilation techniques to get improved initial conditions. Barker *et al.* (2012) showed that the RMSE of modified analyses after the assimilation of satellite radiance data is comparatively less in the middle and lower troposphere. Weng *et al.* (2007) showed that

Department of Environmental Sciences, Central University of Jammu, Jammu and Kashmir, India

***Corresponding Author:** Dinesh Kumar, Department of Environmental Sciences, Central University of Jammu, Jammu and Kashmir, India, E-Mail: dkumarcuj@gmail.com

How to cite this article: Kundan, S., Verma, N., Nabi, Z., Kumar, D. (2022). Satellite radiance assimilation using the 3D-var technique for the heavy rainfall over the Indian region. The Scientific Temper, **13**(2):425-431.

Source of support: Nil

Conflict of interest: None.

Received: 10/11/2022 **Accepted:** 03/12/2022 **Published:** 09/12/2022

the assimilation of atmospheric temperature profiles from Advanced Microwave Sounding Unit-A (AMSU-A) into a Global Forecasting System (GFS) using a hybrid variational scheme (HVAR) had a significant impact on initial hurricane vortex structure, lower-level wind circulation, and temperature field. McNally *et al.* (2006) experimented by assimilating Atmospheric Infra-Red Sounder (AIRS) radiance data and consistently improved the quality of analyses and forecasts. Reale *et al.* (2012) also studied the impact of AIRS on heavy rainfall events, which resulted in improved precipitation forecast skills. Recent studies on the assimilation of additional data into the model's initial condition significantly impacted model predictions. For example, Routray *et al.* (2010) have shown a significant impact on the location, propagation, and development of rain bands related to monsoon depressions by assimilating Doppler weather radar (DWR). Mohanty *et al.* (2012) have highlighted that intense rainfall events could be simulated more realistically by assimilating GTS data. In the Indian context, researchers have recently attempted to simulate thunderstorms and other convective events using high-resolution mesoscale models (Vaidya, 2007; Litta *et al.*, 2012). However, studies have yet to attempt the impact of satellite radiance on thunderstorm simulation.

The present study is an attempt to investigate the impact of satellite radiance data assimilation on the simulation of thunderstorms over the Indian region. Satellite radiance data includes Atmospheric Infra-Red Sounder (AIRS), Advanced Microwave Sounding Unit-A (AMSU-A), Advanced Microwave Sounding Unit-B (AMSU-B), High-resolution InfraRed Sounder-3 (BHRS-3), High-resolution InfraRed Sounder-4 (BHRS-4), and Microwave Humidity Sounder (MHS). It is relevant here to mention that different channels of these datasets (AIRS, AMSU-A & B, HIRS, and MHS) peak at different atmospheric levels. Satellite radiance data is assimilated to improve the initial condition. Four thunderstorm events that occurred over Kolkata on 25 May (cases-1), 31 May (case-2), 4 May (case-3), and 30 May (case-4), 2011, respectively, are considered.

MATERIALS AND METHODS

Modeling System

For the simulation of severe thunderstorms over the Indian region, an ARW model with a 3DVAR analysis system has been used. It is a weather prediction model designed for both research and operational applications. Multiple physics options, nesting domain, and multiple portable platforms make the ARW model flexible enough to be configured to simulate/forecast extreme weather events such as tropical cyclones, heavy rainfall, and severe thunderstorms. Details regarding the model physics option and model equations may be found in Skamarock *et al.* (2005).

The 3D-Var data assimilation system provided in the ARW model allows the WRF model to run with or without data assimilation. This system is based on Bayesian probabilities and Gaussian error distributions (Lorenc, 1986; Lorenc *et al.*, 2000) and provides an estimate of the state of the atmosphere with the help of an iterative solution of a cost function J(x) given by

$$J(x) = J^b + J^o = \frac{1}{2}(x - x^b)^T B^{-1} (x - x^b) + \frac{1}{2}(y - y^o)^T (E + F)^{-1} (y - y^o) \quad (1)$$

where J^b and J^o are the cost functions of background and observation, respectively; x is the state vector; x^b is the background or first guess; B is the background error statistics covariances; y is the observation space (y= Hx); H is the forward (non-linear) operator; y^o is the observations; E is the observational or instrumental error covariances matrix; F is the representativity error covariances matrix. Further details regarding the applications of the 3DVAR system are documented in Barker *et al.* (2004) and Jianfeng *et al.* (2005).

Numerical Experiments

Model configurations, such as model domain, model physics (parameterization schemes), horizontal resolution, etc., are illustrated in this section. Two domains are used; the outer domain of 9 km and the inner nested domain of 3 km horizontal resolution have been used (Figure 1). The outer domain covers 80°E -98°E and 16°N-30°N centered at 89° E, 23° N, while, inner nested domain covers 85˚-93˚E and 20˚–27˚N. Table 1 gives a brief illustration of the model configuration used for the present study. Two numerical experiments, namely CNTL and SAT, were carried out. The control simulation (CNTL) was initialized with National Centers for environmental prediction (NCEP) FiNaL (FNL) analyses data (in 6 hours intervals of 1°× 1° horizontal resolution) without any additional data assimilation. In the assimilation experiment, the model's initial condition was updated by assimilating satellite radiance. A number of quality checks were performed in the preprocessor, including the removal of the observations that were outside of the time range and the domain (horizontal and top), reordering and merging of the duplicate observations using the hydrostatic assumptions and vertical consistency checks,

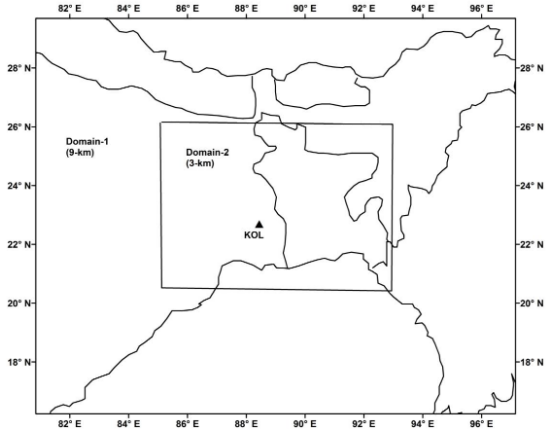

Figure 1: Domain (nested) used for current study

Table 1: Model configuration and physical parameterization used for the present study

Model Configuration		
The time step for Integration	30	
Number of Domains	2	
East-west Dimension	203	295
South-north Dimension	180	232
Vertical Levels	51	
Grid Distance in X-direction in Km	9000	3000
Grid Distance in Y-direction in Km	9000	3000
X-coordinate of the lower left corner	1	53
Y-coordinate of the lower left corner	1	56
Grid ratio	1	3
Physical Parameterization		
Microphysics Option	WSM-6 class Graupel Scheme	
Long wave radiation Option	GFDL (eta) Long wave shortwave radiation option (99)	
Short wave radiation Option	GFDL (eta) Long wave shortwave radiation option (99)	
Land surface Option	NOAH Scheme (2)	
Planetary Boundary option	YSU (1) Mellor-Yamada-Janjic (eta) TKE scheme (2)	
Cumulus Parameterization option	Kain-Fritsch scheme (1) Betts-Miller-Janjic scheme (2) Grell-Devenyi ensemble scheme (3)	

etc. (Barker *et al*., 2004). The model was initialized at 00 UTC and integrated for 24 hours. Model configuration remained the same for CNTL and SAT assimilation experiments. Model simulated rainfall was validated with TRMM accumulated rainfall. The model surface meteorological parameters such as 2 m temperature, and station rainfall were verified against Automatic weather station (AWS) observations, and the model simulated reflectivity was compared with the observed reflectivity of Kolkata Doppler weather radar (DWR).

Data Used

Satellite Radiance

Advanced Microwave Sounding unit-A and B (AMSU-A and AMSUA-B) and high-resolution Infrared Radiation Sounders (HIRS/3 and HIRS/4) from NOAA Polar Orbital Environmental Satellites (POES) were obtained from CISL research data archive (http://rda.ucar.edu/datasets/dssatel) managed by NCAR's data support section. High-Resolution Infrared Radiation Sounders (HIRS/3 and HIRS/4) instruments are infrared sounders that measure the incident radiation primarily in the infrared region of the spectrum in 19 channels. They also have one channel. Its purpose is to measure temperature and water vapor profiles under clear-sky conditions.

Tropical Rainfall Measuring Mission (TRMM)

NASA and JAEA (Japan Aerospace Exploration Agency) made collaborative efforts to monitor and study the rainfall pattern over the tropical region, which is named TRMM. The model simulated rainfall is validated with TRMM (TRMM 3B42-V6) rainfall observations. The TRMM rainfall data has a horizontal resolution of $0.25^o \times 0.25^o$.

Automatic weather station (AWS)

AWS observation is managed and provided by Indian Meteorological Department and is used for hourly monitoring of surface and meteorological variables. AWS data were obtained from the respective IMD regional canter. AWS data were used to validate surface variables such as rainfall and temperature.

Wyoming radiosonde observation

Wyoming radiosonde data were downloaded from the departmental website of the University of Wyoming (http://weather.uwyo.edu/upperair/sounding.html) for the validation of vertical profiles of wind speed, mixing ratio, and equivalent potential temperature. This is sounding data collected over various weather stations situated over different parts of the globe.

Doppler Weather Radar (DWR) observation

DWR data is obtained for the respective dates of case studies from regional centers of IMD, i.e., Kolkata and New Delhi. IMD maintains 14 DWR observations installed at different parts of the country, i.e., Delhi, Mumbai, Kolkata, Chennai, Lucknow, etc. DWR observation monitors the squall lines and frontal precipitation bands in 500 Km periphery. DWR is a type of radar used to locate precipitation, calculate its motion, and estimate its type (rain, snow, hail, etc.).

FNL- Reanalysis-Data

The FNL analyses come from NCEP's Global Data Assimilation System, which runs four times a day in 1^o x 1^o horizontal resolution. In FNL data, the analysis fields serve as initial conditions.

Synoptic conditions of the Convective Events (Thunderstorms)

Case-1, 25 May2011

An examination of plots obtained from NCEP FNL data (Figure 3a) at 00 UTC on 25 May 2011 (Case-1) indicates an elongated low-pressure area that extends from north Pakistan to west Uttar Pradesh and a trough from this running through Bihar and Jharkhand up to Head Bay. An upper air cyclonic circulation over Assam and the neighborhood is seen in lower levels. Another upper-air cyclonic circulation over central Pakistan and adjoining northwest Rajasthan is seen

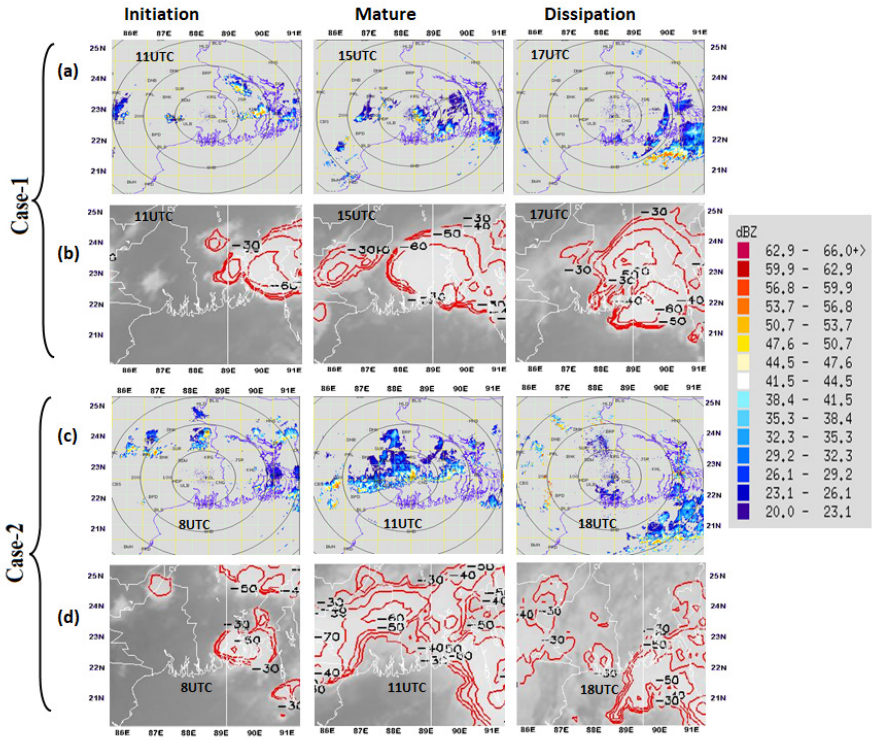

Figure 2: (a) Kolkata DWR and (b) Kalpana (Cloud Top Temperature, CTT) images at different stages (initiation, mature and dissipation) of thunderstorm in Case-1. (c - d) are same as (a–b) but for case-2

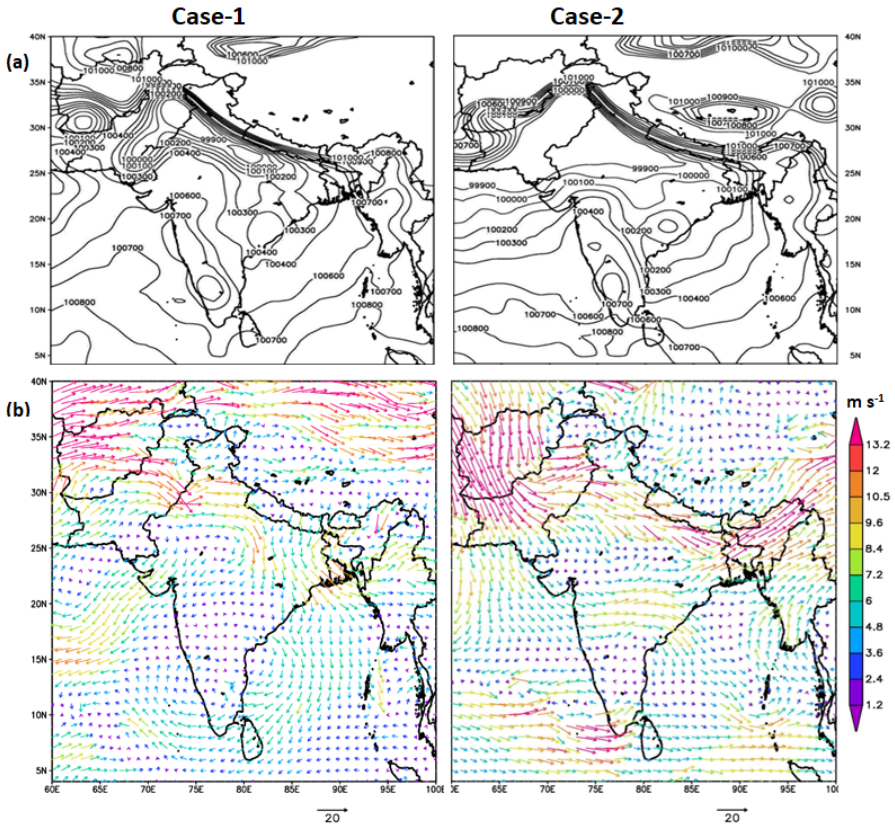

Figure 3: Synoptic plot of (a) surface pressure (b) wind at 500 hPa at 0UTC for case-1 and case-2

in lower levels. A trough from this system extends up to Gangetic West Bengal across Haryana, Uttar Pradesh, and Jharkhand (fig-3b). Another upper air cyclonic circulation lies over Gangetic West Bengal and the neighborhood, which extends up to 3.1 km above mean sea level. Further, a north-south trough from south Chhattisgarh to south Tamil Nadu is observed in the lower levels. The sub-tropical westerly jet stream lies over the Tibetan plateau far north of the study domain. Kalpana satellite imagery (fig-2b) shows convection (Cloud top temperature (CTT) -30°C) developing over Bangladesh and adjoining Tripura. This system intensified and expanded further, covering central and south Bangladesh, adjoining Tripura, Nagaland, and some parts of West Bengal with a CTT of -60°C by 15 UTC. This system merged with another convective cloud cell over West Bengal at 15 UTC. Convective echoes were noticed at about 200-250Km northeast of Kolkata in the images of Doppler Weather Radar (DWR) (Figure 2a) at Kolkata at 11 UTC, which later intensified into a northwest–southeast oriented squall line spanning about 150-200km by 15 UTC. It further moved south/southeastwards and dissipated by 17 UTC. Further, light rain occurred at Kolkata (12.8mm), Canning (18.6mm), Basirhat (19.8 mm), and very light rain occurred at Kalaikunda (3.4mm), Midnapore (1mm), and Kharagpur (1mm).

Case-2, 31 May2011

NCEP FNL derived surface pressure plots (fig-3a) at 00 UTC of 31 May 2011 (Case 2) indicate an elongated low pressure that extends from north Pakistan to west Uttar Pradesh, and a trough from this runs through Bihar up to Bangladesh. A trough runs from Orissa and Adjoining West Bengal to the south peninsula along coastal Andhra Pradesh and Tamilnadu. At 925 hPa, the coastal winds along Orissa and West Bengal are southerly to south-westerly. At 500 hPa, the mid-tropospheric trough lies at 89° E. The sub-tropical westerly jet stream is seen over the Tibetan plateau, which is far north of the area of interest. Kalpana satellite imagery (fig-2d) shows convection (Cloud top temperature (CTT) -30°) developing over Jharkhand and adjoining West Bengal at 08 UTC. These echoes intensified and expanded into a northeast–southwest oriented convective system covering West Bengal, Jharkhand, and north Orissa by 11 UTC. The system weakened and dissipated by 18 UTC.

RESULTS

The model results were analyzed for all four cases to study the above-mentioned data's impact on the simulation of convection associated with thunderstorms. A detailed discussion is presented here for two of the four cases examined in the study. The improvements in initial conditions after the assimilation of satellite radiance are presented first. The impact on model simulations is shown further.

Initial condition results

The improvement in the initial condition was analyzed by taking RMSE of the vertical profile of temperature and specific humidity, increments in mixing ratio, and wind magnitude. Radiosonde observations were used to validate the relative humidity and wind speed vertical profiles initially. The root mean square error (RMSE) of temperature and specific humidity at different model levels is depicted in Fig-4 for Case 1 and Case 2. It was noticed that the SAT experiments showed less RMSE for temperature and specific humidity at all model levels as compared to CNTL experiments. In particular, the improvement is significant in the mid-planetary boundary layer (PBL). Figure 5 shows the spatial distribution of the initial mixing ratio at 850 hPa level. For the CNTL experiment, the actual values of the mixing ratio are shown; however, the spatial increments (i.e., the difference between SAT and CNTL experiments) are shown for case-1 and case-2. Comparing moisture fields in CNTL and SAT experiments, positive increments in the moisture field (1–5 g kg^{-1}) were seen in SAT experiments, particularly over the thunderstorm region. However, the atmosphere to the east and north of the thunderstorm region is relatively drier in SAT experiments (Fig 5 a and b). Similarly, positive increments in wind magnitude in the range of 1.0 – 6.0 m s^{-1} (Fig 5 c and d) were noticed, which is in the region of thunderstorm occurrence in SAT experiment.

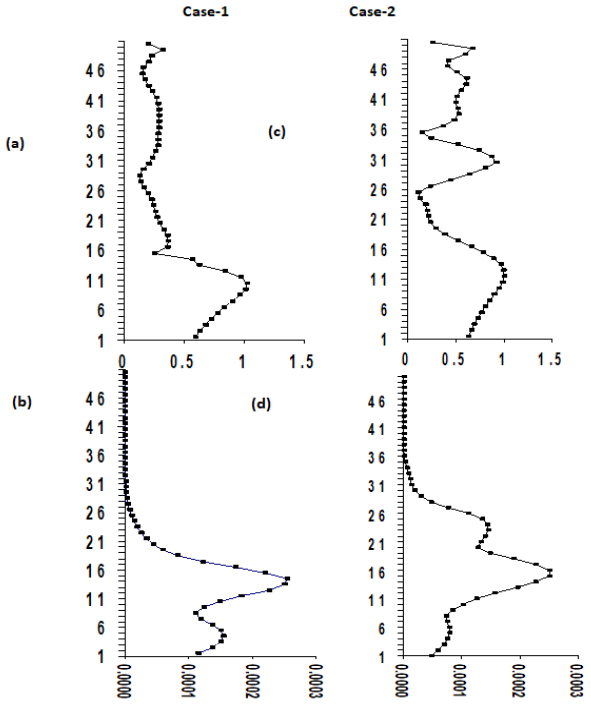

Figure 4: RMSE of (a) temperature, (b) specific humidity at different model vertical levels (Y-Axis) at initial time for case-1. (c – d) are same as (a – b) but for case-2

Model Forecast Results

Fig-6a illustrates the time series of thermodynamic stability indices, i.e., Convective Available Potential Energy (CAPE) for case 1 and case 2 at Kolkata. The observed CAPE was obtained from the FNL analyses. The time series showed that CAPE in SAT experiments was in good agreement with the observed CAPE. In case 1 and case 2, the SAT experiments showed the maximum CAPE of about 3384 J kg−1 and 2766 J kg−1 at 14 UTC and 9 UTC, respectively. Though the CNTL experiments showed CAPE intensity similar to the SAT experiments, the time lag was more. Figure 6c shows the temporal evolution of rainfall for case 1 and case 2, respectively. The observed rainfall is 13 mm at 16 UTC in case-1 and 5 mm at 12 UTC in case 2, respectively. SAT experiment showed the hourly rainfall with a time lag of two hours in case 1 and case 2. Though SAT experiments showed an overestimation of rainfall in case-2, the time lag is significantly reduced as compared to the CNTL experiments. The evolution of the model simulated 2m temperature (Figure 6b) in SAT experiments showed a temperature drop of 7°C and 11°C at 13 UTC and 10 UTC (in case-1 and case-2, respectively), which is closer to AWS observation.

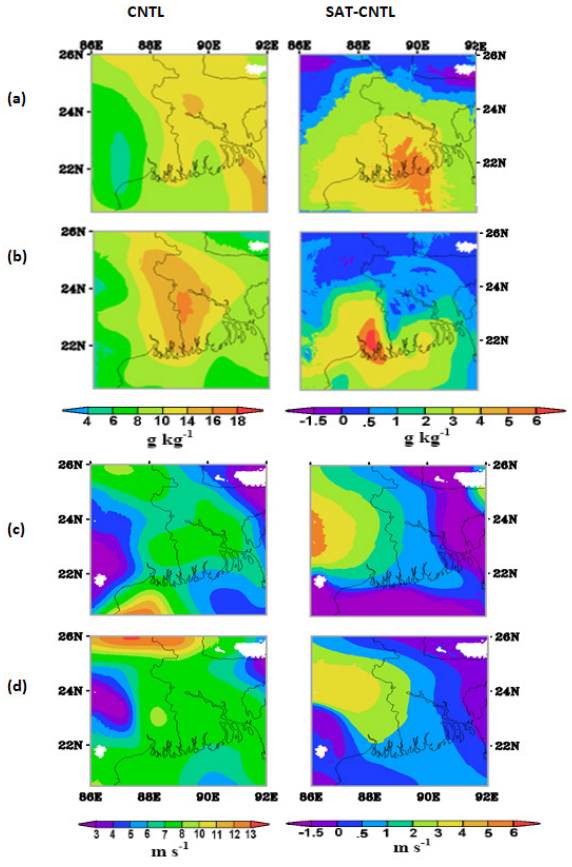

Figure 5: Initial mixing ratio (g kg-1) from CNTL analysis and SAT-CNTL presents the analysis increment of mixing ratio for Case-1. (b) are same as (a) but for Case-2. (c) and (d) are same as (a) and (b) respectively, but for wind magnitude (m/s).

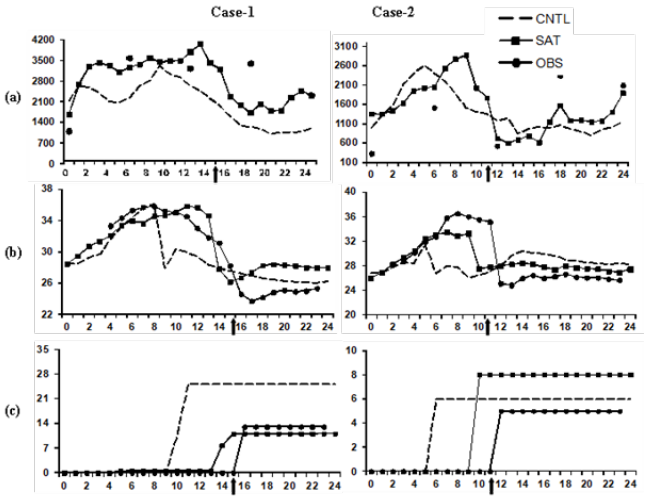

Fig-6: Temporal Evolution of (a) CAPE J kg-1, (b) temperature (°c) and (c) rainfall (mm) for case-1. (d - f) are same as (a - c) but for case-2. Arrow indicates the time of thunderstorm occurrence.

Fig-7 and Fig-8 provide time-height cross-sections of moisture convergence for case 1 and case 2 over Kolkata, respectively. The time-height cross-sections of moisture convergence for case 1 (Figure 7) showed that the moisture convergence in CNTL experiments started to build up from 8UTC and became strong at 9 UTC extending up to about 600 hPa level. The elevated moisture convergence in CNTL experiments was shown much before the observed time of the thunderstorm. However, in the SAT experiments, the moisture convergence build-up was seen closer to the observed time of thunderstorm occurrence. Further, SAT experiments captured two moisture convergence peaks between 13UTC and 16 UTC in case-1 which is closer to the observed (time lag is 2 hours). These two peaks were associated with continuous rainfall in SAT experiments (Figure 6a). Similar results were also found in case 2 in SAT experiments in terms of improved occurrence timing and intensity of thunderstorms.

Figure 6b and Figure 7b show the time-height cross-section of vertical velocity (cm s^{-1}) for case 1 and case 2, respectively. SAT experiments showed a strong updraft (100-400 cm s^{-1}) at 14UTC in case 1 and 10UTC in case-2 (750-400 hPa). Figure 7c and fig-8c show the time-height cross-section f the mixing ratio (g kg-1) for case 1 and case-2, respectively. It was observed that the mixing ratio had increased significantly in SAT experiment at the respective updraft. Further, SAT experiments showed more moisture content, extending vertically up to 750 hPa around 12UTC (case-1) and around 9UTC (case-2).

The CNTL and SAT experiments reflectivity for case 1 and case 2 are presented in Figure 9, and observed reflectivity images of Kolkata DWR are shown in Figure 2. Convective echoes simulated by the SAT and CNTL experiments in case 1 show that the echoes at the respective initiation time were in the same direction as seen in the observed, which is east

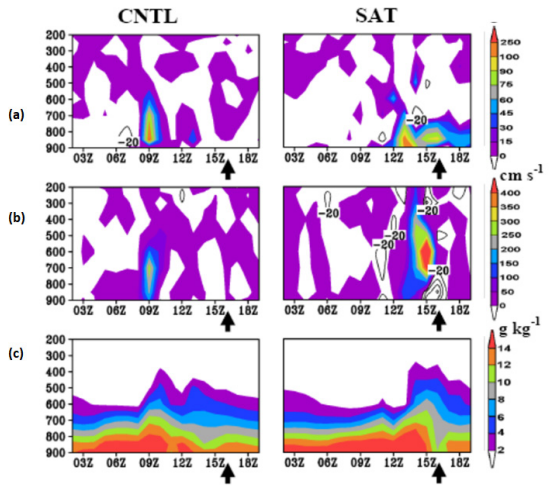

Figure 7: Height-time cross-sections of (a) Moisture Convergence (g kg-1 s-1), (b) Vertical velocity (cm s-1) and (c) Mixing Ratio (g kg-1) for Case-1 over Kolkata. Arrow indicates the time of thunderstorm occurrence.

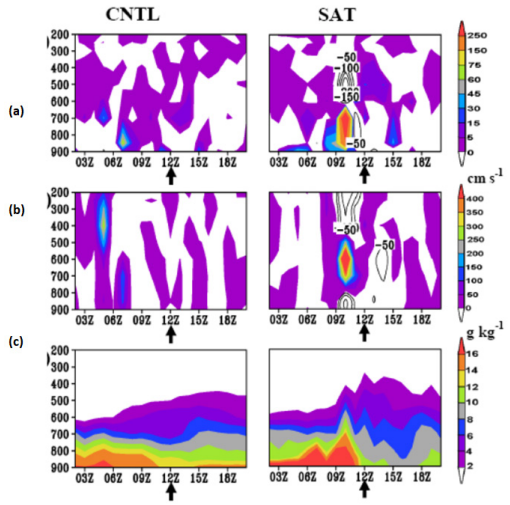

Figure 8: Height-time cross-sections of (a) Moisture Convergence (g kg-1 s-1),(b) Vertical velocity (cm s-1) and (c) Mixing Ratio (g kg-1) for Case-2 over Kolkata. Arrow indicates the time of thunderstorm occurrence.

and northeast of Kolkata. Further, at the mature stage, the squall line orientation and structure were reproduced well in SAT experiments as compared to CNTL experiments. In case-2, the SAT and CNTL experiments simulated convective echoes to the north and northwest of Kolkata, slightly displaced from the observed one. Further, SAT experiments were able to capture the southward movement of the squall line, which was absent in the CNTL experiments.

Six hourly models simulated accumulated rainfall during the thunderstorm occurrence are presented along with TRMM rainfall for all four cases in Figure 10. TRMM observation showed maximum rainfall over Bangladesh in case-1 and case-3, while the maximum rainfall region is located over WB and its boundary and Bangladesh in case-2 and case-4, respectively. Case 1 and case 2 show a maximum

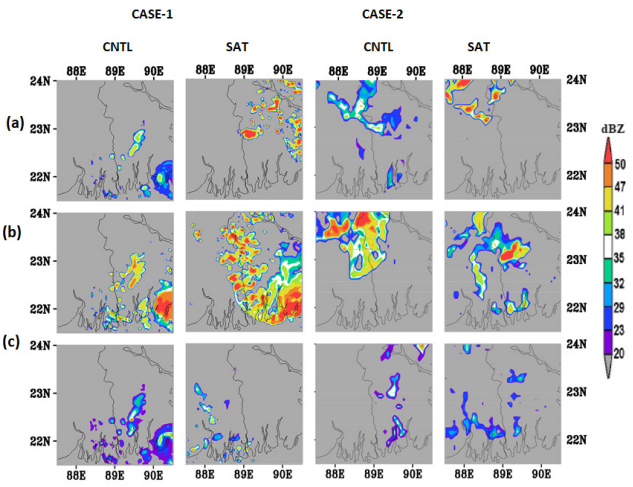

Figure 9: Simulated reflectivity at (a) initiation stage, (b) mature stage, and (c) dissipation stage for case-1 and case-2

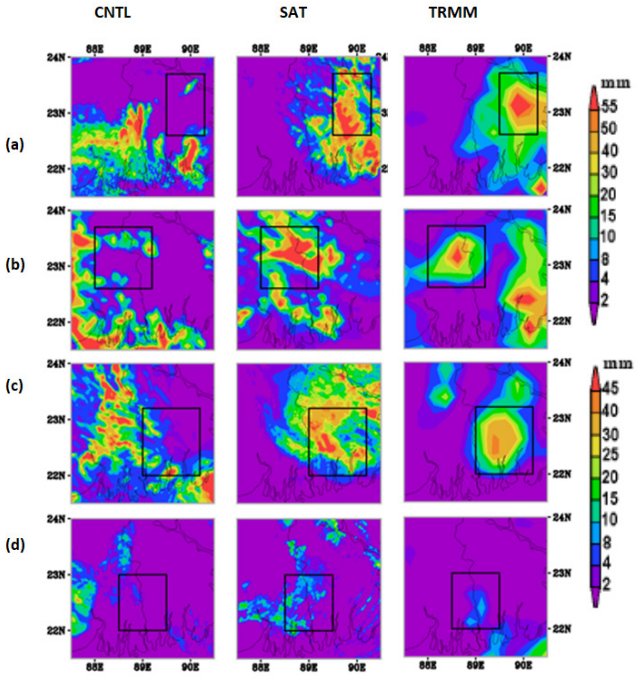

Figure 10: 6-hourly accumulated rainfall (mm) along with TRMM observed rainfall during severe thunderstorm event for (a) case-1 (12UTC-18UTC), (b) case-2 (6UTC-12UTC), (c) case-3 (0UTC-6UTC) and (d) case-4 (0UTC-6UTC).

rain of 55 mm, while 40 mm and 10 mm of rain are seen in case 3 and case 4, respectively. The spatial distribution of the rainfall was seen closer to TRMM observation in SAT experiments than CNTL experiments.

Discussions

Assimilation of satellite radiance significantly affects the initial condition and should improve predictability in terms of associated variables. The discussion of initial condition improvements and impact on the forecast is presented hereafter.

Impact at the initial condition

Satellite radiance assimilation has improved significantly the initial condition, which has led to the realistic evolution of the atmosphere. Accurate initial conditions are considered crucial for the success of the NWP forecast (Lewis *et al*., 1985). Forecast accuracy/error used is most sensitive to initial condition improvement/error, often in cloudy and rainy regions (McNally 2002). To analyze the improvement in the initial condition, RMSE of the vertical profile of temperature and specific humidity, increments in mixing ratio, and wind magnitude were taken at the initial condition. Radiosonde observations have been used to validate the relative humidity and wind speed vertical profiles at the initial condition. In particular, the improvement is significant in the mid-planetary boundary layer (PBL). This may be due to the reason that assimilation of HIRS and AMSU radiance data had improved the moisture content in mid-upper tropospheric levels (English *et al*., 2000). RMSE for temperature and specific humidity have reduced at all model levels after assimilation. Positive increments were seen in the spatial distribution of the initial mixing ratio and wind fields in SAT experiments (i.e., the difference between SAT and CNTL experiments). Further, these positive increments were in agreement with the observed pattern of weather variables such as moisture and wind fields.

Impact on model forecast

Atmospheric instabilities arise in a condition where air masses (temperature and humidity) have density differences which intensify the thunderstorm (Price 2006). Therefore, the model simulated instability indices such as Convective Available Potential Energy (CAPE J/kg) and Lifted Index (LI) are compared with those of available six hourly FNL observations. Other hourly parameters like 2 meters (2m) temperature and rainfall are presented along with AWS observations. CAPE is the amount of buoyant energy to accelerate a parcel vertically. The critical value of CAPE for super-cells to form is >1500 J kg–1 (Rasmussen, 1983). The observed CAPE was obtained from the FNL analyses. Time series showed that CAPE in SAT experiment was in good agreement with the observed CAPE. Thus, SAT has captured the convective atmosphere over Kolkata better and was closer to the actual occurrence of thunderstorms. Further, it is evident that SAT experiments had captured the convective atmosphere over Kolkata better and were closer to the actual occurrence of thunderstorms. Though SAT showed an overestimation of rainfall in case-2, the time lag was significantly reduced as compared to the CNTL experiments. Previous studies have shown that the genesis of thunderstorms involves the significant role of surface parameters (e.g., surface temperature). The temperature at the surface has been found to be a useful parameter in forecasting the occurrence of a thunderstorm (Lopez *et al*., 2007). Improvements in temperature, wind, and moisture fields have led to a better conducive atmosphere which has been reflected in the time series of temperature, rainfall, and thermodynamic stability indices (CAPE).

Analysis of vertical velocity, moisture convergence, and mixing ratio

Time-height cross-sections of moisture convergence are helpful in investigating the availability of moisture in the lower atmosphere. Many previous studies have shown that convective updraft speeds define the intensity of convection. Stronger convective updrafts indicate more intense storms, which carry more ice into anvils and produce more lightning (Zipser *et al*., 2006). On the other hand, downdraft intensity is used for forecasting damaging winds and hazardous wind shear (Kirkpatrick *et al*., 2009). Further, the coexistence of strong updraft and downdraft side by side without mutual coexistence is an indication of severe thunderstorm occurrence. Low-level moisture convergence accompanied by strong upward vertical velocity strengthens the possibility of thunderstorm occurrence in an unstable atmosphere. In the context of the present study, moisture convergence and mixing ratio, along with vertical velocities, became stronger in the SAT experiments. However, moisture convergence increased more significantly in the lower atmosphere in SAT experiments. It was also observed that vertical velocity enhanced in SAT experiments which impacted the CAPE significantly. The experiments result in Analysis indicated that the assimilation had reduced the time lag in SAT experiments when compared with observations. The better results in SAT experiments may be because they simulated an unstable atmosphere with high CAPE at the right time to trigger convection in an improved way. Doppler Weather Radar (DWR) facilitates an in-depth view of mesoscale and near-storm scale structures of various convective events, such as squall lines and frontal precipitation bands, simulated by high-resolution models (Koch *et al*., 2005). SAT experiments were able to capture the southward movement of the squall line, which was not seen in the CNTL experiment. So, it can be inferred that SAT experiments captured the squall lines associated with thunderstorm better as compared to the CNTL experiment.

Rainfall Analysis

Surface precipitation is considered a very important but relatively difficult parameter to predict (Wang and Seaman, 1997), although the accuracy of numerical models has increased significantly during the past several decades. TRMM rainfall has been used to validate the model simulation of six hourly accumulated rainfall. The spatial distribution of the rainfall is simulated closer to TRMM observation in SAT experiment as compared to CNTL experiments. The improved simulation of rainfall in SAT may be due to the better organization of mesoscale moisture convergence with the assimilation of moisture fields from satellite radiance (Abbs, 1999). The overall better representation of

rainfall in SAT may be because of the reduced time lag and better spatial positioning of thunderstorm activity. Results indicate that the assimilation of satellite radiance using the 3D-VAR technique has improved the characteristic features of thunderstorm simulation, which was absent or weaker in the without-assimilation experiment (CNTL). The above discussion suggests that the assimilation of satellite radiance data improves the overall simulations substantially and has the potential to be used effectively in the simulation of thunderstorms in the Indian region.

ACKNOWLEDGMENTS

The author acknowledges the financial support provided by DST-SERB (Project Sanction No-EEQ_2017_000206). We thank the India Meteorological Department (IMD) for providing the observations for model validation. The authors gratefully acknowledge the NCEP/NCAR for providing FNL analyses and satellite radiance datasets for the present study.

REFERENCES

Abbs, D. J. (1999). A numerical modeling study to investigate the assumptions used in the calculation of probable maximum precipitation. Water Resources Research, 35(3), 785–796.

Barker, D. M., Huang, W., Guo, Y. R., Bourgeois, A. J., & Xiao, Q. N. (2004). A three-dimensional variational data assimilation system for MM5: Implementation and initial results. Monthly Weather Review, 132(4), 897–914.

Barker, D., Huang, X. Y., Liu, Z., Auligné, T., Zhang, X., Rugg, S., & Zhang, X. (2012). The weather research and forecasting model's community variational/ensemble data assimilation system: WRFDA. Bulletin of the American Meteorological Society, 93(6), 831-843.

English, S. J., Renshaw, R. J., Dibben, P. C., Smith, A. J., Rayer, P. J., Poulsen, C., ... and Eyre, J. R. (2000). A comparison of the impact of TOVS arid ATOVS satellite sounding data on the accuracy of numerical weather forecasts. Quarterly Journal of the Royal Meteorological Society, 126(569), 2911–2931.

Jianfeng, G. U., Xiao, Q., Kuo, Y. H., Barker, D. M., Jishan, X., & Xiaoxing, M. A. (2005). Assimilation and simulation of typhoon Rusa (2002) using the WRF system. Advances in Atmospheric Sciences, 22, 415–427.

Johns, R. H., and Doswell III, C. A. (1992). Severe local storm forecasting. Wea. Forecasting, 7(4), 588–612.

Kirkpatrick, C., McCaul, E. W., & Cohen, C. (2009). Variability of updraft and downdraft characteristics in a large parameter space study of convective storms. Monthly Weather Review, 137(5), 1550–1561.

Koch, S. E., Ferrier, B., Stoelinga, M. T., Szoke, E., Weiss, S. J., and Kain, J. S. (2005, October). The use of simulated radar reflectivity fields in the diagnosis of mesoscale phenomena from high-resolution WRF model forecasts. In Preprints, 11th Conf. on Mesoscale Processes, Albuquerque, NM, Amer. Meteor. Soc., J4J (Vol. 7, pp. 1-9).

Lewis, J. M., and Derber, J. C. (1985). The use of adjoint equations to solve a variational adjustment problem with advective constraints. Tellus A, 37(4), 309-322

Litta, A. J., Mohanty, U. C., Das, S., & Idicula, S. M. (2012). Numerical simulation of severe local storms over east India using WRF-NMM mesoscale model. Atmospheric Research, pp. 116, 161-184.

López, L., García-Ortega, E., and Sánchez, J. L. (2007). A short-term forecast model for hail. Atmospheric research, 83(2-4), 176-184.

Lorenc, A. C. (1986). Analysis methods for numerical weather prediction. Quarterly Journal of the Royal Meteorological Society, 112 (474), 1177–1194.

Lorenc, A. C., Ballard, S. P., Bell, R. S., Ingleby, N. B., Andrews, P. L. F., Barker, D. M., ... & Saunders, F. W. (2000). The Met. Office global three-dimensional variational data assimilation scheme. Quarterly Journal of the Royal Meteorological Society, 126(570), 2991–3012.

Maussion, F., Scherer, D., Finkelnburg, R., Richters, J., Yang, W., and Yao, T. (2011). WRF simulation of a precipitation event over the Tibetan Plateau, China–an assessment using remote sensing and ground observations. Hydrology and Earth System Sciences, 15(6), 1795-1817.

McNally, A. P. (2002). A note on the occurrence of clouds in meteorologically sensitive areas and the implications for advanced infrared sounders. Quarterly Journal of the Royal Meteorological Society: A Journal of the atmospheric sciences, applied meteorology and physical oceanography, 128(585), 2551–2556.

McNally, A. P., Watts, P. D., A. Smith, J., Engelen, R., Kelly, G. A., Thépaut, J. N., and Matricardi, M. (2006). The assimilation of AIRS radiance data at ECMWF. Quarterly Journal of the Royal Meteorological Society: A Journal of the atmospheric sciences, applied meteorology and physical oceanography, 132(616), 935–957.

Mohanty, U. C., Routray, A., Osuri, K. K., & Kiran Prasad, S. (2012). A study on simulation of heavy rainfall events over Indian region with ARW-3DVAR modeling system. Pure and Applied Geophysics, pp. 169, 381–399.

Mukhopadhyay, P. (2004). Idealized simulation of a thunderstorm over Kolkata using RAMS. *J* Ind Geophys Union, 8(4), 253-266

Narayanan, M. S., Shah, S., Kishtawal, C. M., Sathiyamoorthy, V., Rajeevan, M., & Kriplani, R. H. (2005). Validation of TRMM merges daily rainfall with IMD rain gauge analysis over Indian land mass. Space Appl. Centre, Ahmedabad, India, Tech. Rep.

Orlanski, I. (1975). A rational subdivision of scales for atmospheric processes. Bulletin of the American Meteorological Society, pp. 527-530

Price, C. (2006). Global thunderstorm activity, Sprites. In, Fullekrug, M. *et al.* (Ed.), Sprites, Elves, and Intense Lightning Discharges 1981; 85–99.

Rahman, H., & Sengupta, D. (2007). Preliminary comparison of daily rainfall from satellites and Indian gauge data. CAOS technical report, (2007AS1).

Rasmussen, E. N. (1983). Relationships between storm characteristics and 1200 GMT hodographs, low-level shear, and stability. In Preprints of 13^< th> Conf. on Severe Local Storms, Tulsa, OK, Amer. Meteor. Soc., 1983.

Reale, O., Lau, K. M., Susskind, J., and Rosenberg, R. (2012). AIRS impact on Analysis and forecast of an extreme rainfall event (Indus River Valley, Pakistan, 2010) with a global data assimilation and forecast system. Journal of Geophysical Research: Atmospheres, 117(D8).

Routray, A., Mohanty, U. C., Niyogi, D., Rizvi, S. R. H., & Osuri, K. K. (2010). Simulation of heavy rainfall events over Indian

monsoon region using WRF-3DVAR data assimilation system. Meteorology and atmospheric physics, pp. 106, 107–125.

Skamarock, W. C., Klemp, J. B., Dudhia, J., Gill, D. O., Barker, D. M., Wang, W., and Powers, J. G. (2005). A description of the advanced research WRF version 2. National Center For Atmospheric Research Boulder Co Mesoscale and Microscale Meteorology Div.

Talagrand, O., & Courtier, P. (1987). Variational assimilation of meteorological observations with the adjoint vorticity equation. I: Theory. Quarterly Journal of the Royal Meteorological Society, 113(478), 1311-1328.

Vaidya, S. S. (2007). Simulation of weather systems over Indian region using mesoscale models. Meteorology and atmospheric physics, 95(1-2), 15-26.

Wang, W., and Seaman, N. L. (1997). A comparison study of convective parameterization schemes in a mesoscale model. Monthly Weather Review, 125(2), 252-278.

Weng, F., Zhu, T., & Yan, B. (2007). Satellite data assimilation in numerical weather prediction models. Part II: Uses of rain-affected radiances from microwave observations for hurricane vortex analysis. Journal of the Atmospheric Sciences, 64(11), 3910–3925.

Yin, Z. Y., Zhang, X., Liu, X., Colella, M., & Chen, X. (2008). An assessment of the biases of satellite rainfall estimates over the Tibetan Plateau and correction methods based on topographic Analysis. Journal of Hydrometeorology, 9(3), 301–326.

Zipser, E. J., Cecil, D. J., Liu, C., Nesbitt, S. W., and Yorty, D. P. (2006). Where are the most intense thunderstorms on Earth? Bulletin of the American Meteorological Society, 87(8), 1057-1072.